

Time scales in shear banding of wormlike micelles

O. RADULESCU¹, P. D. OLMSTED², J. P. DECRUPPE³, S. LEROUGE⁴, J.-F. BERRET⁵
and G. PORTE⁵

¹ IRMAR - Université de Rennes1, Campus de Beaulieu, 35042, Rennes, France

² Dept. of Physics and Astronomy, University of Leeds, Leeds LS2 9JT, UK

³ LPLI - Université de Metz, Metz, France

⁴ LLB - CEA-CNRS, Saclay, France

⁵ GDPC - Université de Montpellier II, Montpellier, France

PACS. 47.50.+d – Non-Newtonian fluid flows.

PACS. 83.10.Tv – Rheology, Structural and phase changes.

PACS. 83.80.Qr – Surfactant and micellar systems, associated polymers.

Abstract. – We show the existence of three well defined time scales in the dynamics of wormlike micelles after a step between two shear rates on the stress plateau. These time scales are compatible with the presence of a structured interface between bands of different viscosities and correspond to the isotropic band destabilization during the stress overshoot, reconstruction of the interface after the overshoot and travel of a fully formed interface. The last stage can be used to estimate a stress diffusion coefficient.

Introduction. – Depending on the type and concentration of surfactant molecules and added salt, solutions of surfactant wormlike micelles have shear thinning or thickening behavior under shear flow. Unlike most fluids, wormlike micelles often have non-analytic flow curves with sharply-selected plateaus along which strain rate or stress may change discontinuously. In the well documented case of shear thinning solutions the usual explanation of the constant stress plateau is shear banding [1, 3, 2], *i.e.* a separation of the material into bands of different viscosities, triggered by a constitutive instability (such as an isotropic-to-nematic transition [2]). As shown recently [8, 9, 10, 11, 12], the stress selection and history independence of shear banding can be explained using the inhomogeneities of the relevant mesoscopic order parameter (polymer stress), *i.e.* by incorporating “diffusive” terms in the constitutive equations. Order parameter diffusion was introduced long time ago by van der Waals in the so-called “gradient theory” of the gas-liquid interface [7], and is obligatory in phase field models for pattern formation. Notwithstanding a few attempts to deal with inhomogeneous stresses [6] the same concept has not obtained full acceptance in the rheological community. While one might argue that diffusion terms are negligibly small, these *non-perturbative* terms resolve stress selection even for infinitesimal values [11]. However, a small diffusion coefficient should also imply a slow approach to steady state; the main purpose of this letter is to demonstrate these long time scales experimentally and relate them to simple model diffusive behavior.

TABLE I – *Surfactant systems used in this study; the surfactant was 0.3 M CTAB. τ and G_0 , are the Maxwell relaxation time and plateau modulus, $\dot{\gamma}_I, \delta\dot{\gamma}$ are the start and width of the constant stress plateau, $(\tau_i)_{i=1,3}$ are the three time scales discussed in the text, and σ^* is the plateau stress.*

No.	Salt	T [°C]	G_0 [Pa]	τ [s]	τ_1 [s]	τ_2 [s]	τ_3 [s]	$\tau\dot{\gamma}_I$	$\tau\delta\dot{\gamma}$	σ^*/G_0
1	1.79M <i>NaNO</i> ₃	30	232	0.17	0.2	2.4	30.6	0.85	19	0.64
2	0.405M <i>NaNO</i> ₃	30	238	0.17	0.2	1.8	25	1.27	19	0.66
3	0.3M <i>KBr</i>	34	235	0.16	0.2	3.7	9.3	1.12	80	0.66

Shear banding involves spatial inhomogeneity and several temporal stages. Light polarization probes the local micellar orientation, while rheology detects the molecular stress. In this work we shall calculate the stress transients using a theoretical model. This will be compared to birefringence measurements that are assumed to probe the state of molecular orientation and hence stress (but see Ref. [13]) Rather than the typical start-up transient experiment, we consider the simpler experiment of a step between two fixed values of the shear rate in the banded regime. Small steps should induce less drastic changes in the fluid while still remaining in the non-linear regime, and hopefully yield more controllable results. The transient features will be shown to be intimately related to the dynamics of the interface between the bands.

Experiments. – The surfactant solutions used are summarized in Table I. The stress response was measured using an RFS Rheometrics Scientific controlled strain rate rheometer in Couette (radii 24.5, 25 mm) and cone-plate geometries. Linear response is of the Maxwell type with almost identical relaxation times τ and moduli G_0 for the three solutions. In the non-linear regime the coexistence plateau width $\delta\dot{\gamma}$ for solution 3 is larger than for solutions 1 and 2, while solutions 1 and 2 have a sloped stress plateau that roughly follows a power law $\sigma \sim \dot{\gamma}^\alpha$, with $\alpha \lesssim 0.1$; a slope could indicate concentration differences between coexisting states [14]. Upon a step increase of the shear rate between banded states the stress increases to a maximum, and then decreases monotonically (or sometimes by a small undershoot and a monotonic increase). Three relaxation times ($\tau_1 \approx \tau \approx 10^{-1}$ s, $\tau_2 \approx 10\tau \approx 1$ s and $\tau_3 \approx 100\tau \approx 10$ s) follow successively after the overshoot until steady flow is reached (Fig. 1a). The

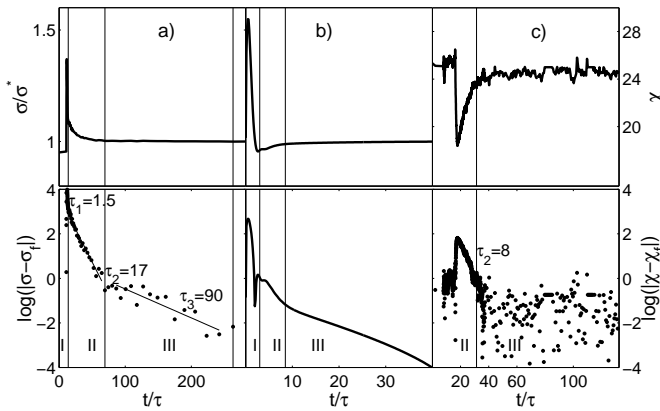


Fig. 1 – Stages and characteristic times (in τ units): a) total stress during the step $\dot{\gamma} = 10 \rightarrow 20$ s^{-1} for CTAB/KBr; b) simulated total stress during the step $\dot{\gamma} = 1.4/\tau \rightarrow 2.8/\tau$ using the d-JS model; c) Extinction angle during the step $10 \rightarrow 20$ s^{-1} for CTAB/KBr.

three time scales are well separated and the result is reproducible for all solutions and both cone-plate and Couette geometries. We filmed the step shear rate experiment for the third solution in a Couette geometry with a slightly larger gap (radii 24, 25 mm) between crossed polarizers to extract the average extinction angle χ . The kinetics of χ resemble that of the shear stress, displaying time scales similar to the second and the third time scales found in the rheology (Fig. 1c). The first, unresolvable, time scale is shorter than the interval between successive video frames. The second time scale is well resolved, although shorter by a factor of two than the equivalent time in the stress rheology measurements. The third time scale is buried in noise and regression does not provide significant results.

Theory. – The momentum balance is $\rho(\partial_t + \mathbf{v} \cdot \nabla) \mathbf{v} = \nabla \cdot \mathbf{T}$, where ρ is the fluid density and \mathbf{v} is the velocity field. The stress tensor \mathbf{T} is given by $\mathbf{T} = -p\mathbf{I} + 2\eta\mathbf{D} + \boldsymbol{\Sigma}$, where the pressure p is determined by incompressibility ($\nabla \cdot \mathbf{v} = 0$), η is the “solvent” viscosity, $\boldsymbol{\Sigma}$ is the “polymer” stress, and \mathbf{D} is the symmetric part of the velocity gradient tensor $(\nabla \mathbf{v})_{\alpha\beta} \equiv \partial_\alpha v_\beta$. The non-Newtonian “polymer” viscoelastic stress $\boldsymbol{\Sigma}$ is assumed to obey the diffusive Johnson-Segalman (d-JS) model [9],

$$(\partial_t + \mathbf{v} \cdot \nabla) \boldsymbol{\Sigma} - (\boldsymbol{\Omega} \boldsymbol{\Sigma} - \boldsymbol{\Sigma} \boldsymbol{\Omega}) - a(\mathbf{D} \boldsymbol{\Sigma} + \boldsymbol{\Sigma} \mathbf{D}) = \mathcal{D} \nabla^2 \boldsymbol{\Sigma} + 2\mu \mathbf{D} / \tau - \boldsymbol{\Sigma} / \tau, \quad (1)$$

where $\boldsymbol{\Omega}$ is the anti-symmetric part of $\nabla \mathbf{v}$, $\mu = G_o \tau$ is the “polymer” viscosity, τ is a relaxation time, and \mathcal{D} is the diffusion coefficient. The “slip parameter” a (describing the non-affinity of the deformation) is necessary to reproduce a non-monotonic constitutive curve, and the added diffusion term was shown to resolve stress selection [9].

The initial dynamics is governed by inertia; within a very short time $\tau_M = \rho L^2 / \eta$ ($\tau_M = 10^{-4}$ s for $\eta / \rho = 0.01 \text{ m}^2 \text{ s}^{-1}$ and a gap $L = 1$ mm) momentum diffuses across the gap and the momentum balance becomes $\mathbf{T} = \text{const}$. The subsequent slower dynamics is controlled by the viscoelastic response of the fluid. In a planar geometry with $\mathbf{v} = v(y)\hat{\mathbf{x}}$, our constitutive model leads to a system of reaction-diffusion equations⁽¹⁾:

$$\frac{\partial S}{\partial t} = \mathcal{D} \frac{\partial^2 S}{\partial y^2} - \frac{S}{\tau} + C_S(\dot{\gamma}, S, W), \quad \frac{\partial W}{\partial t} = \mathcal{D} \frac{\partial^2 W}{\partial y^2} - \frac{W}{\tau} + C_W(\dot{\gamma}, S, W), \quad (2)$$

where $\dot{\gamma}$ is the shear rate, $S = \Sigma_{xy}$, and W is a combination of the polymer normal stresses, Σ_{xx} and Σ_{yy} . S, W are the order parameters of the transition (S is small in the nematic (N) band, and large in the isotropic (I) band). They can diffuse across stream lines with diffusion coefficient \mathcal{D} , and relax in the linear regime within the linear (Maxwell) time τ . The non-linear reaction terms $C_S = \dot{\gamma}(G_o - W)$ and $C_W = \dot{\gamma}S$ can be straightforwardly derived from Eq. (1) [8, 10].

The local momentum balance for the shear stress $\sigma = T_{xy}$ is

$$\sigma = S + \epsilon G_o \tau \dot{\gamma}, \quad (3)$$

where $\epsilon = \eta / \mu$. The dynamics of Eq. 2 can be understood with the aid of two (local) dynamical systems:

$$\dot{S} = -S/\tau + C_S(\dot{\gamma}, S, W), \quad \dot{W} = -W/\tau + C_W(\dot{\gamma}, S, W); \quad (4a)$$

$$\dot{S} = -S/\tau + C_S((\sigma - S)/\epsilon G_o \tau, S, W), \quad \dot{W} = -W/\tau + C_W((\sigma - S)/\epsilon G_o \tau, S, W) \quad (4b)$$

⁽¹⁾Any non-monotonic differential constitutive model (*e.g.* Cates [17], Doi-Edwards [16, 15]) with diffusion terms leads to a similar equation set.

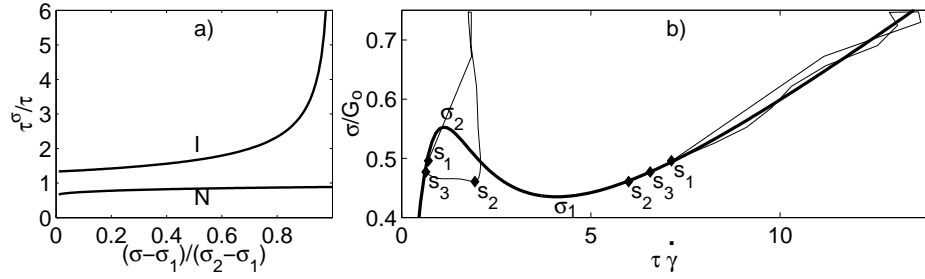


Fig. 2 – a) Relaxation times to I and N attractors at constant stress, $\tau_I^\sigma, \tau_N^\sigma$. b) Thick line: theoretical flow curve (the negative slope, unstable branch should be replaced by the constant stress plateau). Thin lines: trajectories of the coexisting bands near the walls. $\{s_i\}, i = 1, 3$ are the starting points of the three stages discussed in the paper.

where $\dot{S} \equiv \partial S / \partial t$. System (4a) describes the dynamics along a streamline at prescribed shear rate; in this case σ changes proportionately to S according to Eq. (3). System (4b) describes the dynamics along a streamline at constant total stress σ .

The two dynamical systems have the same fixed points (since, for homogeneous steady flow, $\dot{\gamma}$ and σ are related by Eq. 3): stable fixed points (attractors) representing the bands I and N, and an intermediate unstable saddle fixed point. Coexistence of bands at common total stress is possible only for $\sigma \in [\sigma_1(\epsilon), \sigma_2(\epsilon)]$. Linearizing systems (4a) and (4b) about the fixed points yields the dominant relaxation times of the attractors, τ_I and τ_N . These are different for the two dynamical systems, denoted at constant shear rate by $\tau_{I,N}^\dot{\gamma}$ and at constant stress by $\tau_{I,N}^\sigma$. For the JS model $\tau_I^\dot{\gamma} = \tau_N^\dot{\gamma} = \tau$ for all $\dot{\gamma}$. τ_N^σ is close to τ , while τ_I^σ is larger than τ_N^σ and diverges as $\sigma \rightarrow \sigma_2(\epsilon)$ (Fig. 2a). This divergence is consistent with Ref. [5]: controlled stress experiments have much longer relaxation times on the metastable extension of the high viscosity branch above the constant stress plateau.

Consider an initial banded steady state, with average shear rate $\langle \dot{\gamma} \rangle$. Suddenly increasing the average shear rate to $\dot{\gamma}_2 > \langle \dot{\gamma} \rangle$ produces a stress overshoot because the amount of high viscosity I band is too large; both I and N bands then become unstable, and the stress can decrease by producing more of the low viscosity N material. Numerical simulation (Figs. 1, 3) shows that this occurs in three stages:

1. *Band I destabilization*— During this stage the I band tries a direct passage toward the nematic band N, (Fig. 3a). Complete transformation is forbidden by the average shear rate constraint and the I band stops before reaching the basin of attraction of the steady N band. A representation of the subsequent kinetics in the $(\dot{\gamma}, \sigma)$ plane (Fig. 2b) shows that *the N band almost follows the steady flow curve, while the I band evolves at constant shear rate*. Thus, the characteristic time $\tau_1 \approx \tau_I^\dot{\gamma} \approx \tau$ is controlled by the I band dynamics. The total shear stress at the end of this stage depends on the final position of the interface and is sensitive to the details of the constitutive model. If this value is below the plateau one finds an undershoot (as in the numerical simulation Fig. 1b), and otherwise the subsequent stress evolution is monotonic (Fig. 1a). Although we did not succeed in reproducing monotonic evolution using the JS model, as long the I band evolves at a constant shear rate, the magnitude of the characteristic time should not be affected by the presence or absence of an undershoot.

2. *Interface reconstruction*— At the end of stage 1 the interface separates an unsteady I band close to the unstable saddle point from a nearly stable N band. The part of the profile closer to the I attractor will evolve toward this one, while the other part approaches the N

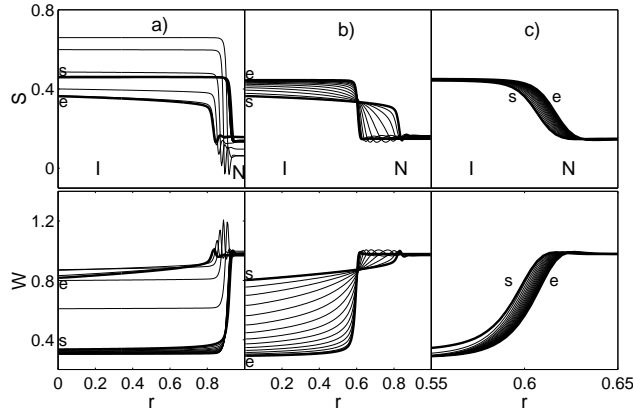


Fig. 3 – Simulation of the order parameter profiles for the three stages (s: start, e: end): a) destabilization ($0 < t < t_1$); b) reconstruction ($t_1 < t < t_2$); c) travel ($t_2 < t < \infty$).

attractor. This reconstructs the interface in a more advanced position, stabilizes the bands, and increases the contrast between them. Interestingly, there is a spatial position at which S and W practically remain fixed at their saddle fixed point values. During this stage $\langle \dot{\gamma} \rangle$ is constant (because it is imposed) and $\langle S \rangle$ is almost constant (because of the compensating evolutions of the two bands), so according to Eq. (3) the total stress variation is small, and the characteristic time (controlled by the I band) is $\tau_2 \approx \tau_I^\sigma$. This time exceeds the linear viscoelastic time τ (see Fig. 2), and depends on how close the stress at the end of stage 1 is to the spinodal limit $\sigma_2(\epsilon)$, and on the quantitative details of the curve in Fig. 2, all of which are sensitive to the constitutive model. The analysis suggested by the numerical experiment is confirmed by the birefringence measurements. The sequence of images in Fig. 4 show the gap of the Couette cell filmed between crossed polarizers during stage 2. Although we can not quantitatively compare Figs. 3b) and 4 (the relation between the transmitted intensity and the order parameter is unknown and sure to be non-linear), the sharpening of the contrast corresponding to the interface reconstruction is visible. The difference between the characteristic times for the extinction angle and rheology (Fig.1) could be due to the different Couette cell gap widths.

3. *Interface travel*— The instability and reconstruction of the interface in the first two stages is ensured by the reaction terms of the Eq. (2), ending when a sharp interface between stable bands is fully formed. This interface could have a non-zero velocity if it forms in at a position corresponding to a stress value above or below the plateau stress σ^* . “Front propagation” over the small distance toward the final equilibrium position is then controlled by \mathcal{D} (this distance is too small to observe by birefringence). Because of the undershoot in the numerical simulation the sign of the displacement during stage 3 is opposite to the one in the first stages (Fig.3c). The characteristic time τ_3 for this stage follows from the velocity c of the sharp interface close to steady state which is independent of the presence or absence of the undershoot [10] (see below).

Let us consider a single sharp interface, at a position r inside the gap. At imposed shear rate, the lever rule $\langle \dot{\gamma} \rangle = \frac{r}{L} \dot{\gamma}^N(\sigma) + (1 - \frac{r}{L}) \dot{\gamma}^I(\sigma)$ relates σ and r and leads to

$$\left(\frac{\partial \sigma}{\partial r} \right)_{\langle \dot{\gamma} \rangle} = \frac{-\eta_I \delta \dot{\gamma}}{L[1 + (\langle \dot{\gamma} \rangle - \dot{\gamma}^I) / \dot{\gamma}^I]}, \quad (5)$$

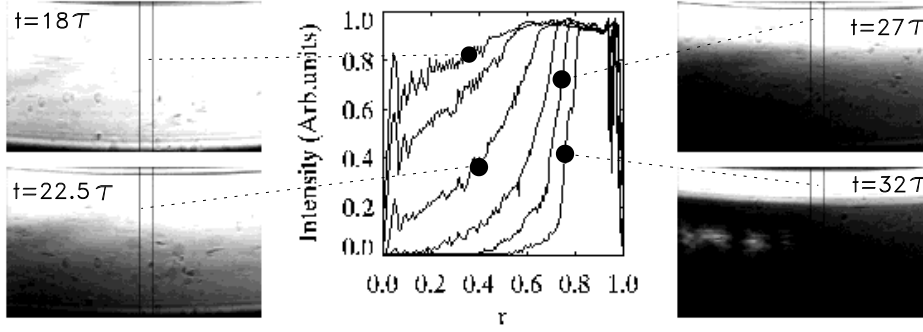


Fig. 4 – CTAB/KBR: $\dot{\gamma} = 10 \rightarrow 30\text{s}^{-1}$ jump: birefringence images and profiles (averaged between the two vertical lines on the film) corresponding to the second time scale, showing the interface reconstruction. The moving (inner) cylinder is at $r = 1.0$ and the fixed (outer) cylinder is at $r = 0.0$.

where $\delta\dot{\gamma} = \dot{\gamma}_N - \dot{\gamma}_I$ is the width of the plateau, and $\eta_I = \partial\sigma/\partial\dot{\gamma}|_{\dot{\gamma}_I}$. We consider $\langle\dot{\gamma}\rangle - \dot{\gamma}_I \ll \delta\dot{\gamma}$, $\delta\dot{\gamma} \gg \dot{\gamma}_I$ (as in the experiments) so that $\eta^I \dot{\gamma}^I \approx \eta^N \delta\dot{\gamma}$ (true for piecewise linear flow curves and obeyed well by the JS model).

We showed previously that the velocity c of the interface is a function of the total shear stress σ only, and that $c = 0$ when $\sigma = \sigma^*$ [8, 10] which via the lever rule corresponds to a unique stable interface position r_* . Thus, close to this position r_* the equation of motion of the interface is:

$$\frac{dr}{dt} = c(\sigma) = \frac{dc}{d\sigma} \left(\frac{\partial\sigma}{\partial r} \right)_{\langle\dot{\gamma}\rangle} (r - r_*). \quad (6)$$

Using Eqs. (5,6), and the derivative $\frac{d\sigma}{dc}|_{\sigma=\sigma^*} \equiv KG_o\sqrt{\frac{\tau}{\mathcal{D}}}$, we find the solution $r - r_* = (r(0) - r_*)e^{-t/\tau_3}$, with characteristic time

$$\tau_3 = K \frac{L}{\sqrt{\mathcal{D}\tau}} \frac{1 + [\langle\dot{\gamma}\rangle - \dot{\gamma}_I]/\dot{\gamma}_I}{\delta\dot{\gamma}}, \quad (7)$$

where the dimensionless constant K depends on the particular constitutive model.

Eq. (7) implies that a fully formed interface equilibrates faster in systems with larger plateaus $\delta\dot{\gamma}$, such as CTAB/KBr. In such cases, Eq. (5) implies larger stress variations and thus larger interface accelerations for the same position variation. This is compatible with the shorter τ_3 in Table I. For simplicity, Eq. (5) was for a planar geometry; in cylindrical Couette flow a slight correction (negligible for the thin gaps we consider) leads to a smaller τ_3 .

Using the experimental value of τ_3 and Eq. 7, we can estimate \mathcal{D} . In order to do this we need the value of K . In the JS model, while G_0 and τ are measurable, the two free parameters ϵ and a determine the function K . Nevertheless, $\tau G_o \delta\dot{\gamma}/\sigma^* = f_1(\epsilon)$, $\dot{\gamma}_I/\delta\dot{\gamma} = f_2(\epsilon)$ and $K/(\tau\delta\dot{\gamma}) = f_3(\epsilon)$ are functions of ϵ only, given to a good approximation ($> 80\%$) by $f_1(\epsilon) = \frac{4}{3\epsilon} \sqrt{\frac{1/8-\epsilon}{1/2-\epsilon}}$, $f_2(\epsilon) = \frac{3\epsilon}{\sqrt{(1-8\epsilon)(1-2\epsilon)+1-8\epsilon}}$, $f_3(\epsilon) = \frac{3}{8}\epsilon^2 f_1(\epsilon)$. From either f_1 , or f_2 and experimental data, one can estimate ϵ (the average of the two values is given in Table II) and then f_3 gives K (Table II). Thus we do not need the value of a . Microscopically, we expect $\mathcal{D} = \zeta^2/\tau$ where ζ is the stress correlation length. In dilute solutions this should be the micelle gyration radius [6], while in concentrated solutions a reasonable candidate is the

TABLE II – *Stress diffusion estimates using the JS model. \mathcal{D} is obtained from the values of τ_3 (table I) and Eq. 7 with ϵ, K estimated using $\dot{\gamma}_I$ and $\delta\dot{\gamma}$.*

Sample	L [mm]	$(\dot{\gamma} - \dot{\gamma}_I)/\dot{\gamma}_I$	ϵ	K	\mathcal{D} [$m^2 s^{-1}$]	ζ [nm]	ξ [nm]
1	0.3	4	0.023	0.10	$11 \cdot 10^{-15}$	44	26
2	0.3	2.33	0.028	0.12	$11 \cdot 10^{-15}$	43	26
3	0.3	1.85	0.007	0.14	$3 \cdot 10^{-15}$	22	26

mesh size ξ , which can be estimated from $G_o \sim kT/\xi^3$. The results are presented in Table II. The stress correlation length is of order the mesh size, which is reasonable; however there is still no theory for such a diffusive term in concentrated solutions.

To conclude, a general dynamical systems analysis of the d-JS model provides plausible explanations for the observed time scales, and consistent estimates of the stress diffusion coefficient \mathcal{D} . Nevertheless, neither the d-JS model, nor reptation-retraction-reaction models [16, 17] can provide perfect fits of transient stress curves in the nonlinear regime. Also, it is conceivable that concentration differences between the bands could influence the observed time scales. The difference of the values of \mathcal{D} between samples 1,2 and 3 (Table II) could be a concentration effect, consistent with the different slopes of the flow curves plateaus (tilted for 1,2, almost horizontal for 3).

* * *

We thank J.-F. Tassin for his kind assistance and for allowing our access to the rheometer facilities of Université du Maine. O.R. acknowledges funding from EU COST Action P1 on Soft Condensed Matter and from EPSRC (GR/L70455) at the beginning of this work.

REFERENCES

- [1] REHAGE H. and HOFFMANN H. , *J. Phys.Chem.*, **92** (1988) 4712.
- [2] BERRET J.-F., ROUX D. C. and PORTE G., *J. Phys. II (France)*, **4** (1994) 1261.
- [3] SPENLEY N. A., CATES M. E., AND MCLEISH T. C. B., *Phys. Rev. Lett.*, **71** (1993) 939.
- [4] BERRET J.-F., *Langmuir*, **13** (1997) 2227.
- [5] GRAND C., ARRAULT J. and CATES M. E., *J. Phys. II (France)*, **7** (1997) 1071.
- [6] EL-KAREH A. W. and LEAL L. G., *J. Non-Newtonian Fluid Mech.*, **33** (1989) 257.
- [7] VAN DER WAALS J. D., *Verh. Konink. Akad. Wetensch. Amsterdam*, **1** (1893) 1071, translated in ROWLINSON J. S., *J. Stat. Phys.*, **20** (1979) 197.
- [8] RADULESCU O., OLMSTED P. D. and LU C.-Y. D., *Rheol. Acta*, **38** (1999) 606.
- [9] OLMSTED P. D., RADULESCU O. and LU C.-Y. D., *J. Rheol.*, **44** (2000) 257.
- [10] RADULESCU O. and OLMSTED P. D. , *J. Non-Newtonian Fluid Mech.*, **91** (2000) 141.
- [11] LU C.-Y. D., OLMSTED P. D. and R. C. BALL, *Phys. Rev. Lett.*, **84** (2000) 642.
- [12] YUAN X. F, *Europhys. Lett.*, **46** (1999) 542; DHONT J., *Phys. Rev.*, **E60** (1999) 4534.
- [13] FISCHER E., AND CALLAGHAN P. T., *Europhys. Lett.*, **50** (2000) 803.
- [14] SCHMITT V., MARQUES, C. M., and LEQUEUX, F., *Phys. Rev.*, **E52** (1995) 4009; OLMSTED P. D. and LU C.-Y. D., *Phys. Rev.*, **E56** (1997) 55.
- [15] LARSON R. G., *Constitutive Equations for Polymer Melts and Solutions* (Butterworth, Guildford) 1988.
- [16] DOI M. and EDWARDS S. F., *The Theory of Polymer Dynamics* (Clarendon, Oxford) 1986.
- [17] CATES M. E. , *J. Phys. Chem.*, **94** (1990) 371.